Topological features and properties associated with development/decay of vortices in isotropic homogeneous turbulence

K. Nakayama*
Department of Mechanical Engineering, Aichi Institute of Technology, Toyota, Aichi 470-0392, Japan
(Received 16 May 2016; published 6 January 2017)

Topological features of vortices in terms of local flow geometry in an isotropic homogeneous turbulence and relationships between the topology and development of a vortex are investigated. Swirlity and sourcity represent the unidirectionality and intensities of the azimuthal and radial flows, respectively. Skewness reflects the symmetry quantity of the vortical flow. Together, the three quantities characterize the details of the invariant flow geometry. The analysis shows that flow symmetry is correlated with swirlity, and associated with its development or decay, especially for weak vortices. Stronger vortices exhibit lower correlations between the two and lack sufficient flow symmetry for inflow in all directions. This clarifies why highly intense vortices cannot attain effective vortex stretching. Vortex stretching is formulated in terms of the radial flow in the swirl plane. It shows that stretching is not entirely characterized by the eigenvalues of the rate-of-strain tensor, and depends on the eigenvalues of the radial flow classified by sourcity. Sourcity shows that numerous vortices, which have been classified as inflow (convergent) vortices using the complex eigenvalues of the velocity gradient tensor, have a mixture of inflow and outflow. These vortices break the orthogonality of the vortical axis to the swirl plane during vortex stretching. Stretching in vortices with complete inflow increases vorticity normal to the swirl plane effectively and improves axis orthogonality. Sourcity classifies these characteristics, and flow symmetry and sourcity are important quantities for effective stretching. The present topological analysis provides important details of vortical flow features in turbulent flows or realistic vortex models, and sourcity extracts the specific vortical region supported by the flow geometry itself.

DOI: 10.1103/PhysRevFluids.2.014701

I. INTRODUCTION

Vortices are associated with many fluid phenomena at various scales, as is evident in their appearance in various turbulences and fluid engineering fields from huge power plants to micro-scale objects. Clarification of such vortical flow phenomena is not only of great interest in fluid dynamics but also important in many fluid engineering techniques. An important characteristic of a vortex with swirling flow is its stability or development arising from its flow geometry (topology). A flow symmetry is associated with this stability of the vortex [1]. Also, vortex stretching [2,3] is a particular feature that strengthens the vorticity of swirling by an inflowing motion in the swirl plane. Hence, it is important to specify the detailed vortical flow geometry and its relationships to the development/decay of a vortex.

Previous studies in terms of the vorticity vector and rate-of-strain tensor gave useful findings stating that the vorticity vector tends to align with the eigenvector of the intermediate eigenvalue of the rate-of-strain tensor in isotropic homogeneous turbulence or shear flow [3–5]. The characteristics of the vortex stretching in isotropic homogeneous turbulence have also been investigated in detail [3], and it has been shown that intense vortices (high vorticity region) do not attain sufficient vortex stretching even though the rate-of-strain tensors have similar intensities. Furthermore, the eigenvalues of the velocity gradient tensor $\nabla \boldsymbol{v}$ have aided in a classification of the local flow geometry

*nakayama@aitech.ac.jp

or flow pattern that is Galilean invariant, and have been applied to analyze the topological features of vortices in different turbulence settings such as the mixing layer [5] and channel flow [6]. The eigenvalues have also been applied to an important vortex definition of the Δ definition [7] or other identification methods of a vortex or vortical axis [8–14]. The complex eigenvalues of $\nabla \boldsymbol{v}$, say $\varepsilon_R \pm i\psi$ (i: imaginary unit), specify the invariant swirling motion, and the sign of ε_R has been used to classify the vortex as inflow (convergent, stable) or outflow (divergent, unstable) [7,8], and the second and third invariants of $\nabla \boldsymbol{v}$ can be substituted in this classification.

Despite the contribution of these valuable studies, the feature of vortical flow symmetry is unexplained. The details of topological analysis to complement it have been sought [6], and complex eigenvalues have been used in the lack of their precise physical interpretation. Recently, this interpretation and supplemental topological quantities has been derived by investigating the local velocity specified by $\nabla \boldsymbol{v}$ decomposing into the radial and azimuthal velocities, v_r and v_θ, in a plane. v_r and v_θ are expressible as specific quadratic forms [15], and characteristics of the their eigenvalues specify ε_R and ψ. The algebraic condition of the complex eigenvalues of $\nabla \boldsymbol{v}$ (the Δ definition) is equivalent to the geometrical condition that v_θ has the same direction, and it also shows that both inflow and outflow may exist irrespective of the sign of ε_R. Then several physical quantities were defined that specify unidirectionality of v_r and v_θ, and vortical flow symmetry (skewness). One of symmetry quantities is associated with the pressure minimum feature in the swirl plane in a unified vortex definition of the Δ, Q [16], and λ_2 [17] definitions [18,19].

The present paper investigates the characteristics of the detailed vortical flow geometry with these quantities described above, and the relationship between the flow geometry and development/decay of a vortex in terms of an intensity of swirling, i.e., swirlity [15]. We analyze vortices in isotropic homogeneous decaying turbulence with low Reynolds number, as a principal feature of a vortex. The joint probability density functions (JPDFs) are used for the analysis in accordance with the previous topological studies [3–6], including time derivatives of the quantities. The analysis shows that the vortical flow symmetry is strongly associated with the swirlity and its development/decay especially in weak vortices. A vortex prefers the increase of the symmetry rather than increase of vorticity only by becoming a skewed vortex.

Moreover, vortex stretching in terms of the enstrophy production is expressed by a formulation with respect to the swirl plane. It clarifies the detailed effect of the stretching in the swirl plane and its normal direction, and shows that the eigenvalues of the rate-of-strain tensor may exaggerate the effect. Importantly, besides the enhancement of swirling, the stretching increases or decreases the orthogonality of a vortical axis to the swirl plane due to the effect in the plane, this feature being categorized by sourcity [15] that specifies the uniformity and intensity of v_r. This study also details why high-intensity vortices do not have a strong or effective vortex stretching supporting the flow geometry itself.

II. INVARIANTS SPECIFYING THE VORTICAL FLOW GEOMETRY

We introduce the physical quantities (invariants) used in the present study that characterize the intensities of swirling, radial flow in all directions, and symmetry [15]. The local flow geometry around a point given by coordinates x_i ($i = 1,2,3$), where the local velocity is expressed as $dx_i/dt = (\partial v_i/\partial x_j)x_j$, can be specified by the eigenvalues and eigenvectors of $\nabla \boldsymbol{v}$ at the point in terms of Galilean invariance [7]. Note that the summation convention is used throughout. Since $\nabla \boldsymbol{v}$ has at least one real eigenvalue ε_a with corresponding eigenvector $\boldsymbol{\xi}_a$, we consider the flow geometry in an arbitrary plane linearly independent of (not parallel to) $\boldsymbol{\xi}_a$. In an (arbitrary) coordinate system $\tilde{x}_i$ ($i = 1,2,3$) where the point is the origin in which the $\tilde{x}_3$ axis is parallel to $\boldsymbol{\xi}_a$ and the $\tilde{x}_1$-$\tilde{x}_2$ plane is the considered plane, the components of $\nabla \boldsymbol{v}$ form a matrix, $\tilde{\boldsymbol{A}} \equiv [\tilde{a}_{ij}] \equiv [\partial \tilde{v}_i/\partial \tilde{x}_j]$ $(i,j = 1,2,3)$, which has the feature that $\tilde{a}_{13} = \tilde{a}_{23} = 0$ and $\tilde{a}_{33} = \varepsilon_a$ because the $\tilde{x}_3$ axis is the invariant subspace of $\nabla \boldsymbol{v}$. We focus on the velocity $\hat{\boldsymbol{v}} = (\hat{v}_1, \hat{v}_2)$ in the $\tilde{x}_1$-$\tilde{x}_2$ plane, i.e., $\hat{v}_i = \tilde{a}_{ij}\tilde{x}_j$ $(i,j = 1,2)$, and decompose it into its azimuthal and radial components, v_θ and v_r, respectively. Note that $\hat{\boldsymbol{v}} = v_r \boldsymbol{e}_r + v_\theta \boldsymbol{e}_\theta$,

where $\boldsymbol{e}_r = 1/|\hat{\boldsymbol{x}}|(\tilde{x}_1,\tilde{x}_2)$ and $\boldsymbol{e}_\theta = 1/|\hat{\boldsymbol{x}}|(-\tilde{x}_2,\tilde{x}_1)$, $\hat{\boldsymbol{x}} = (\tilde{x}_1,\tilde{x}_2)$, and $|\hat{\boldsymbol{x}}| = \sqrt{\tilde{x}_i\tilde{x}_i}$ $(i = 1,2)$. Then v_θ is expressed as

$$v_\theta = \frac{1}{|\hat{\boldsymbol{x}}|}{}^t\hat{\boldsymbol{x}}\,\boldsymbol{Q}_\theta\hat{\boldsymbol{x}}, \tag{1}$$

$$\boldsymbol{Q}_\theta = \begin{bmatrix} \tilde{a}_{21} & -(\tilde{a}_{11}-\tilde{a}_{22})/2 \\ -(\tilde{a}_{11}-\tilde{a}_{22})/2 & -\tilde{a}_{12} \end{bmatrix}, \tag{2}$$

where the superscript t before a vector denotes its transpose. The eigenvalues λ_{θ_i} $(i = 1,2; \lambda_{\theta_1} \leqslant \lambda_{\theta_2})$ of $\boldsymbol{Q}_\theta$ are given as $\lambda_{\theta_1},\lambda_{\theta_2} = (\tilde{a}_{21}-\tilde{a}_{12})/2 \pm \sqrt{(\tilde{a}_{11}-\tilde{a}_{22})^2+(\tilde{a}_{12}+\tilde{a}_{21})^2}/2$. If the signs of λ_{θ_i} are the same, then v_θ is unidirectional around the considered point and hence indicates a swirling flow. Importantly, the condition $\lambda_{\theta_1}\lambda_{\theta_2} > 0$, i.e., $|\boldsymbol{Q}_\theta| > 0$, is equivalent to the algebraic condition for the complex eigenvalues of $\nabla\boldsymbol{v}$ (the Δ definition [7]) specifying the invariant swirling motion expressed by the inequality: $\Delta = (Q/3)^3 + (R/2)^2 > 0$, where Q and R represent the second and third invariants of $\nabla\boldsymbol{v}$, respectively. Thus $\Delta > 0$ is equivalent to the condition that flow swirls in an arbitrary plane independent of (not parallel to) $\boldsymbol{\xi}_a$. Calculating $\lambda_{\theta_1}\lambda_{\theta_2}$ yields the following equation:

$$\lambda_{\theta_1}\lambda_{\theta_2} = Q + \frac{3}{4}\varepsilon_a^2. \tag{3}$$

Here "swirlity" ϕ is defined as

$$\phi = \mathrm{sgn}\big(\lambda_{\theta_1}\lambda_{\theta_2}\big)\sqrt{\big|\lambda_{\theta_1}\lambda_{\theta_2}\big|}, \tag{4}$$

where $\mathrm{sgn}(y)$ denotes the sign of $y \in \mathbf{R}$. ϕ represents the uniformity (or nonuniformity) of the direction of v_θ and the intensity of the geometrical average of λ_{θ_i} $(i = 1,2)$. If $\phi < 0$ $(\lambda_{\theta_1}\lambda_{\theta_2} < 0)$, the azimuthal flow is not unidirectional around the point.

Similar to v_θ, v_r can be expressed also as $v_r = {}^t\hat{\boldsymbol{x}}\,\boldsymbol{Q}_r\hat{\boldsymbol{x}}/|\hat{\boldsymbol{x}}|$ where $\boldsymbol{Q}_r$ is equal to the rate-of-strain tensor in the plane. The eigenvalues λ_{r_i} $(i = 1,2; \lambda_{r_1} \leqslant \lambda_{r_2})$ of $\boldsymbol{Q}_r$ are given as $\lambda_{r_1},\lambda_{r_2} = (\tilde{a}_{11}+\tilde{a}_{22})/2 \pm \sqrt{(\tilde{a}_{11}-\tilde{a}_{22})^2+(\tilde{a}_{12}+\tilde{a}_{21})^2}/2$, and the two eigenvectors $\boldsymbol{\zeta}_{r_i}$ $(i = 1,2)$ of λ_{r_i} are orthogonal. The inflowing (outflowing) motion in all directions is specified by $\lambda_{r_1}\lambda_{r_2} = |\boldsymbol{Q}_r| > 0$. "Sourcity" σ represents the uniformity and intensity of the radial flow as a geometrical average, and is defined as

$$\sigma = \mathrm{sgn}\big(\lambda_{r_1}\lambda_{r_2}\big)\sqrt{\big|\lambda_{r_1}\lambda_{r_2}\big|}. \tag{5}$$

If $\sigma < 0$, v_r is not unidirectional and has both inflowing and outflowing motion, that is, inflowing motion appears in the $\pm\boldsymbol{\zeta}_{r_1}$ direction, and outflowing motion in the $\pm\boldsymbol{\zeta}_{r_2}$ direction.

In vortical flows for which $0 < \phi$, i.e., $0 < \Delta$, $\nabla\boldsymbol{v}$ has a pair of complex conjugate eigenvalues $\varepsilon_R \pm i\psi$ $(\psi > 0)$ and one real eigenvalue (ε_a), their respective eigenvectors being $\boldsymbol{\xi}_{pl} \pm i\boldsymbol{\eta}_{pl}$, and $\boldsymbol{\xi}_a$. Then the flow trajectory can be represented as $\boldsymbol{x} = 2e^{\varepsilon_R t}\{\boldsymbol{\xi}_{pl}\cos(\psi t) - \boldsymbol{\eta}_{pl}\sin(\psi t)\} + e^{\varepsilon_a t}\boldsymbol{\xi}_a$, where the local flow swirls with an angular velocity ψ in the plane defined by $\boldsymbol{\xi}_{pl}$ and $\boldsymbol{\eta}_{pl}$, hereafter referred to as the swirl plane $\mathcal{P}$, and proceeds (or approaches) along a vortical axis $\boldsymbol{\xi}_a$. $\boldsymbol{\xi}_{pl}$ and $\boldsymbol{\eta}_{pl}$ can be orthogonal, i.e., $\boldsymbol{\xi}_{pl}\perp\boldsymbol{\eta}_{pl}$. It is noted that, the ratio of their lengths, i.e., $\alpha = |\boldsymbol{\xi}_{pl}|/|\boldsymbol{\eta}_{pl}|$, are specified by the eigenequations of $\boldsymbol{A}$: $\boldsymbol{A}(\boldsymbol{\xi}_{pl} \pm i\boldsymbol{\eta}_{pl}) = (\varepsilon_R \pm i\psi)(\boldsymbol{\xi}_{pl} \pm i\boldsymbol{\eta}_{pl})$.

In the $\tilde{x}_i$ coordinate system, we set the unit bases of the $\tilde{x}_i$ $(i = 1,2)$ axes, $\tilde{\boldsymbol{e}}_1$ and $\tilde{\boldsymbol{e}}_2$, parallel to $\boldsymbol{\xi}_{pl}$ and $\boldsymbol{\eta}_{pl}$, respectively, so that the $\tilde{x}_1$-$\tilde{x}_2$ plane is $\mathcal{P}$, that is, the invariant subspace of $\nabla\boldsymbol{v}$. Then $\tilde{\boldsymbol{A}}$ can be expressed in the form

$$\tilde{\boldsymbol{A}} = \begin{bmatrix} \varepsilon_R & \alpha\psi & 0 \\ -\psi/\alpha & \varepsilon_R & 0 \\ 0 & 0 & \varepsilon_a \end{bmatrix}. \tag{6}$$

We note that $|\tilde{a}_{12}| \neq |\tilde{a}_{21}|$ except when $|\boldsymbol{\xi}_{pl}| = |\boldsymbol{\eta}_{pl}|$ ($\alpha = 1$). λ_{θ_i} ($i = 1,2$) in $\mathcal{P}$, say $\breve{\lambda}_{\theta_i}$, are expressed as the invariant

$$\breve{\lambda}_{\theta_1}, \breve{\lambda}_{\theta_2} = -\psi/c, \ -c\psi = \omega_s \pm \sqrt{\omega_s^2 - \psi^2}, \tag{7}$$

where $c = \alpha$ ($\alpha < 1$) or $1/\alpha$ ($1 \leqq \alpha$), and $\omega_s = -(\alpha + 1/\alpha)\psi/2$. ω_s denotes the component of the vorticity tensor corresponding to $\mathcal{P}$, and is associated with the eigen-helicity density defined by Zhang [14]. Clearly, $\lambda_{\theta_1}\lambda_{\theta_2} > 0$ and $\phi = \psi$, thus ϕ is identical to the swirling strength parameter [11] if $0 < \Delta$. However, ϕ is defined for both vortical and nonvortical flows, and can indicate a transition into vortical flow [20].

In contrast, for v_r, λ_{r_i} ($i = 1,2$) in $\mathcal{P}$, say $\breve{\lambda}_{r_i}$, and σ are given as

$$\breve{\lambda}_{r_1}, \breve{\lambda}_{r_2} = \varepsilon_R \pm \frac{1}{2}\left|c - \frac{1}{c}\right|\psi, \tag{8}$$

$$\sigma = \mathrm{sgn}(\iota)\sqrt{|\iota|}, \tag{9}$$

$$\iota = \varepsilon_R^2 - \frac{1}{4}\left(c - \frac{1}{c}\right)^2 \psi^2. \tag{10}$$

That is, $\breve{\lambda}_{r_i}$ and σ are also given by invariants. Importantly, although the sign of ε_R has been interpreted as classifying a convergent (inflowing) or divergent (outflowing) vortex behavior [7,8], ε_R denotes the arithmetic mean of $\breve{\lambda}_{r_i}$, i.e., $\varepsilon_R = (\breve{\lambda}_{r_1} + \breve{\lambda}_{r_2})/2$. Therefore, it cannot distinguish unidirectional radial flow from mixed inflow and outflow [15]. Hereafter we use the terms "average-inflow (outflow) vortices" for those classified by the sign of ε_R, and "whole-inflow (outflow) vortices" for those classified by ε_R satisfying $0 < \sigma$.

The ratios of λ_{θ_i} ($i = 1,2$) and of λ_{r_i} are associated with the respective flow symmetry of the azimuthal and radial flows in $\mathcal{P}$. α (c) is associated with both symmetries, and hence the whole vortical flow symmetry. Importantly, the local vortical flow geometry differs depending on α even though $\nabla \boldsymbol{v}$ has the same complex eigenvalues, as shown in Fig. 1. The two orthogonal eigenvectors $\boldsymbol{\zeta}_{\theta_i}$ ($i = 1,2$) of λ_{θ_i} can be specified as $\boldsymbol{\zeta}_{\theta_1} = \tilde{\boldsymbol{e}}_2$ ($\boldsymbol{\zeta}_{\theta_1} \parallel \boldsymbol{\eta}_{pl}$) and $\boldsymbol{\zeta}_{\theta_2} = -\tilde{\boldsymbol{e}}_1$ ($\boldsymbol{\zeta}_{\theta_2} \parallel \boldsymbol{\xi}_{pl}$). The directions of $\boldsymbol{\zeta}_{r_i}$ ($i = 1,2$) are given by rotating $\tilde{\boldsymbol{e}}_i$ ($i = 1,2$) in $\pi/4$ clockwise, e.g., $\boldsymbol{\zeta}_{r_1} = 1/\sqrt{2}(1,-1)$ and $\boldsymbol{\zeta}_{r_2} = 1/\sqrt{2}(1,1)$.

It is emphasized that, although past studies of the flow geometry (topology) using Q and R or the vorticity have not considered α (c), this quantity is necessary to specify the flow geometry uniquely. α is defined in $(0,\infty)$, thus c ($0 < c \leqslant 1$) is a normalized quantity of α that represents the flow symmetry or skewness, although the direction of the skewness is lacked. As c changes from 0 to 1, the deformed vortical flow geometry becomes symmetrical. In the present analysis, c is applied as a quantity for the flow symmetry.

III. VORTEX STRETCHING

The vortex stretching term as enstrophy production in the vorticity equation, say δ, can be expressed as $\delta = {}^t\boldsymbol{\omega}\boldsymbol{S}\boldsymbol{\omega} = \omega_i s_{ij} \omega_j$ where $\boldsymbol{\omega} = [\omega_i]$ and $\boldsymbol{S} = [s_{ij}]$ ($i,j = 1,2,3$) denote the vorticity vector and the rate-of-strain tensor, respectively [2,3]. We derive the representation of δ in terms of λ_{r_i} and ε_a. First, we consider a representation of $\nabla \boldsymbol{v}$ in an orthonormal coordinate system $\breve{x}_i$ ($i = 1,2,3$) with bases $\breve{\boldsymbol{e}}_i$ ($i = 1,2,3$) where $\breve{\boldsymbol{e}}_1$ and $\breve{\boldsymbol{e}}_2$ are parallel to $\boldsymbol{\xi}_{pl}$ and $\boldsymbol{\eta}_{pl}$, respectively. Then $\nabla \boldsymbol{v}$ ($= \breve{\boldsymbol{A}} = [\breve{a}_{ij}]$) can be expressed in the form

$$\breve{\boldsymbol{A}} = \begin{bmatrix} \varepsilon_R & \alpha\psi & \breve{a}_{13} \\ -\psi/\alpha & \varepsilon_R & \breve{a}_{23} \\ 0 & 0 & \varepsilon_a \end{bmatrix}. \tag{11}$$

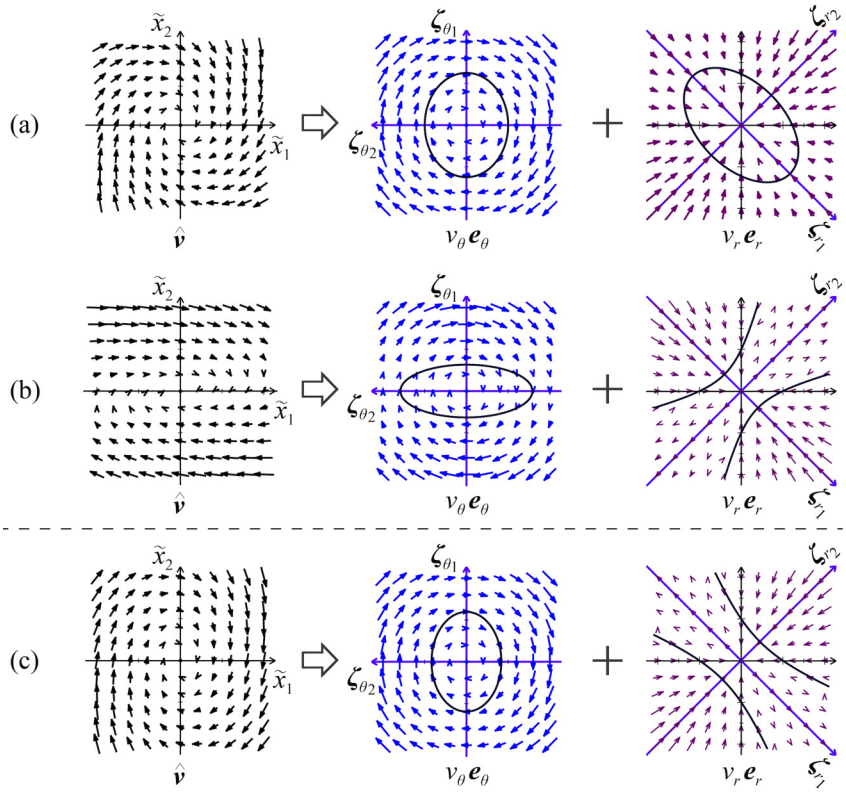

FIG. 1. Flow motions ($\hat{\boldsymbol{v}}$) in $\mathcal{P}$ and decomposed $v_\theta \boldsymbol{e}_\theta$ and $v_r \boldsymbol{e}_r$ with contours of ${}^t\hat{\boldsymbol{x}}\,\boldsymbol{Q}_\theta\hat{\boldsymbol{x}}$ and ${}^t\hat{\boldsymbol{x}}\,\boldsymbol{Q}_r\hat{\boldsymbol{x}}$. (a) and (b) show the flows with the same eigenvalues $(\varepsilon_R, \psi) = (-1, 2)$ but different c where (a) $c = 0.8$ $(=\alpha)$ and $\sigma \approxeq 0.89$, and (b) $c = 0.4$ $(\alpha = 2.5)$ and $\sigma \approxeq -1.85$. (c) a representative flow of an intense vortex where $|\psi/\varepsilon_R| = 4$ $(\varepsilon_R < 0)$, $c = 0.8$, and $\sigma \approxeq -1.1$. Note that for clarity the vector lengths are adjusted in their respective figures.

Note that $\boldsymbol{\xi}_a$ is not orthogonal to $\mathcal{P}$ (not parallel to $\check{\boldsymbol{e}}_3$) in general, and thus $\check{a}_{13}, \check{a}_{23} \neq 0$. $\check{a}_{13}$ and $\check{a}_{23}$ can be expressed in terms of $\boldsymbol{\omega}$ in this coordinate system, $\check{\boldsymbol{\omega}} = [\check{\omega}_i]$ $(i = 1,2,3)$, i.e., $\check{a}_{13} = \check{\omega}_2$ and $\check{a}_{23} = -\check{\omega}_1$. $\check{\omega}_1$ and $\check{\omega}_2$ are given by $\boldsymbol{\xi}_{pl}$ and $\boldsymbol{\eta}_{pl}$: $\check{\omega}_1 = (\boldsymbol{\omega}, \boldsymbol{\xi}_{pl})/|\boldsymbol{\xi}_{pl}|$ and $\check{\omega}_2 = (\boldsymbol{\omega}, \boldsymbol{\eta}_{pl})/|\boldsymbol{\eta}_{pl}|$. When $\check{\omega}_1 = \check{\omega}_2 = 0$, then $\check{a}_{13} = \check{a}_{23} = 0$ and therefore $\boldsymbol{\xi}_a \perp \mathcal{P}$. λ_{θ_i} and λ_{r_i} $(i = 1,2)$ in the $\check{x}_1$-$\check{x}_2$ plane, $\check{\lambda}_{\theta_i}$ and $\check{\lambda}_{r_i}$, are the same as those given by Eqs. (7) and (8).

We consider another orthonormal coordinate system $\hat{x}_i$ $(i = 1,2,3)$ where the bases $\check{\boldsymbol{e}}_1$ and $\check{\boldsymbol{e}}_2$ are rotated in $\mathcal{P}$ by $\pi/4$ clockwise, so that the two bases are identical to $\boldsymbol{\zeta}_{r_i}$ $(i = 1,2)$. $\boldsymbol{S}$ in this coordinate system, $\hat{\boldsymbol{S}} = [\hat{s}_{ij}]$ $(i, j = 1,2,3)$, is expressed in the form

$$\check{\boldsymbol{S}} = \begin{bmatrix} \check{\lambda}_{r_1} & 0 & \hat{a}_{13}/2 \\ 0 & \check{\lambda}_{r_2} & \hat{a}_{23}/2 \\ \hat{a}_{13}/2 & \hat{a}_{23}/2 & \check{\lambda}_{r_3} \end{bmatrix}, \tag{12}$$

where $\hat{a}_{13} = (\check{a}_{13} - \check{a}_{23})/\sqrt{2}$, $\hat{a}_{23} = (\check{a}_{13} + \check{a}_{23})/\sqrt{2}$, and $\check{\lambda}_{r_3} = \varepsilon_a$. Then δ is expressed simply as

$$\delta = \check{\lambda}_{r_1}\hat{\omega}_1^2 + \check{\lambda}_{r_2}\hat{\omega}_2^2 + \check{\lambda}_{r_3}\hat{\omega}_3^2, \tag{13}$$

where $\hat{\omega}_i$ $(i = 1,2,3)$ are the vorticity vector components in this $\hat{x}_i$ coordinate system and $\hat{\omega}_1 = (\check{\omega}_1 - \check{\omega}_2)/\sqrt{2}$, $\hat{\omega}_2 = (\check{\omega}_1 + \check{\omega}_2)/\sqrt{2}$, and $\hat{\omega}_3 = \check{\omega}_3 = 2\omega_s$. Equation (13) is a formulation of δ in terms of the local vortical flow geometry and its swirl plane, and expressed by $\check{\lambda}_{r_i}$ and ε_a. The

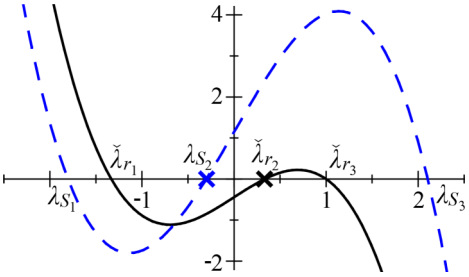

FIG. 2. Characteristics of $\Psi_{\check{S}}(\lambda)$ (line) and Φ_S (dashed line), where $[\check{\lambda}_{r_i}] = (-4/3,1/3,1)$, $(\hat{\omega}_1,\hat{\omega}_2) = (2.4,2)$, $\sigma = -2/3$, and $[\lambda_{s_i}] = (-1.8,-0.3,2.1)$. Note that $\lambda_{s_2} < 0$ but $0 < \check{\lambda}_{r_2}$. If $\hat{\omega}_1 = \hat{\omega}_2 = 0$, then $\Psi_{\check{S}}(\lambda) = \Phi_S$.

associated quantities are then neither the norm $\hat{s}_{ij}\hat{s}_{ij}$ nor eigenvalues of $\boldsymbol{S}$, but the eigenvalues of v_r in $\mathcal{P}$ and real eigenvalue of $\nabla \boldsymbol{v}$.

We clarify the relationship between $\check{\lambda}_{r_i}$ and the eigenvalues of $\boldsymbol{S}$, λ_{s_i} $(i = 1,2,3; \lambda_{s_1} \leqslant \lambda_{s_2} \leqslant \lambda_{s_3})$. The eigenequation of $\boldsymbol{S}$ in terms of $\check{\boldsymbol{S}}$, $\Phi_{\check{S}}(\lambda)$, can be expressed as follows:

$$\Phi_{\check{S}}(\lambda) = \Psi_{\check{S}}(\lambda) - \frac{1}{4}\hat{\omega}_1^2\left(\check{\lambda}_{r_1} - \lambda\right) - \frac{1}{4}\hat{\omega}_2^2\left(\check{\lambda}_{r_2} - \lambda\right), \tag{14}$$

where $\Psi_{\check{S}}(\lambda) \equiv (\check{\lambda}_{r_1} - \lambda)(\check{\lambda}_{r_2} - \lambda)(\check{\lambda}_{r_3} - \lambda)$. Equation (14) depends on $\hat{\omega}_1$ and $\hat{\omega}_2$ ($\check{\omega}_1$ and $\check{\omega}_2$). Moreover, it indicates $\Phi_S(\check{\lambda}_{r_1}) < 0$ and $\Phi_S(\check{\lambda}_{r_2}), \Phi_S(\check{\lambda}_{r_3}) > 0$. Then λ_{s_i} satisfy $\lambda_{s_i} < \check{\lambda}_{r_i}$ $(i = 1,2)$ and $\check{\lambda}_{r_3} \leqslant \lambda_{s_3}$, which indicates that the intensities of the compression and vortex stretching are smaller than the eigenvalues of $\boldsymbol{S}$. More importantly, even if the two eigenvalues of $\boldsymbol{S}$ are negative, i.e., $\lambda_{s_2} < 0$, there are two types of the vortex stretching: (i) stretching with compression in $\mathcal{P}$ (inflow; $\check{\lambda}_{r_1}, \check{\lambda}_{r_2} < 0$) and (ii) stretching with a combination of compression (inflow; $\check{\lambda}_{r_1} < 0$) and stretching (outflow; $0 < \check{\lambda}_{r_2}$) in $\mathcal{P}$. Figure 2 illustrates this feature of two negative eigenvalues for $\boldsymbol{S}$ where both compression (inflow) and stretching (outflow) in $\mathcal{P}$ exist.

IV. NUMERICAL ANALYSIS

The vortices in isotropic homogeneous decaying turbulence are analyzed using the pseudospectral method in a region $(2\pi)^3$ composed of 256^3 nodes. For the wavenumber vector $\boldsymbol{k} = (k_1,k_2,k_3)$, $|k| < 121$ where $|k| = (k_i k_i)^{1/2}$, and the phase shifting method is used for dealiasing [21]. The time step is 0.001 in the fourth-order Runge-Kutta method. An energy spectrum $E(k) = (k/k_p)^4 \exp\{-2(k/k_p)^2\}$ $(k = |k|, k_p = 4)$ [13] gives the initial velocity field with random phases of k, with settings for the (initial) Taylor-Reynolds number $\mathrm{Re}_\lambda = 311$, Taylor microscale $\lambda_T = 0.59$, Kolmogorov length $\eta = 0.015$, and eddy turnover time $t_{\mathrm{eddy}} = 1.14$. The kinetic viscosity is 0.002. ϕ, ε_R, and σ, and other physical quantities are nondimensionalized by their root mean square values in the corresponding time. δ and the components of the vortex stretching $\check{\lambda}_{r_i}\hat{\omega}_i^2$ in Eq. (13) $(i = 1,2,3)$ are divided by $|\omega|^2$ and nondimensionalized by the root mean square value of the vorticity [3], and they are expressed as δ' and $\check{\lambda}'_{r_i}\hat{\omega}_i^2$ ($\varepsilon'_a\hat{\omega}_3^2$ for $i = 3$) to denote the rate of the enstrophy production.

Figure 3 shows the characteristics of the JPDFs associated with $|\omega|$, $|s|$ and δ' in $\mathrm{Re}_\lambda \approxeq 35,51$ after the peak of the enstrophy, where $|\omega|$ and $|s|$ denote $\sqrt{\omega_i\omega_i}$ and $\sqrt{s_{ij}s_{ij}}$, respectively, nondimensionalized by their respective root mean squares. δ' increases only slightly with higher values of $|\omega|$ despite $|s|$ and $|\omega|$ being of the same order with $|s|$ being higher.

These JPDFs of $(|\omega|,|s|)$ and $(|\omega|,\delta')$ in both Re_λ are very similar, as well as being similar to those analyzed by Jiménez *et al.* [3]. Hereafter we show the JPDFs of several quantities where $\mathrm{Re}_\lambda \approxeq 35$. The JPDF of $|\omega|$ and ϕ is shown in Fig. 4, which indicates that a high vorticity region is one with swirling for which $0 < \phi$ or $0 < \Delta$. Thus the identification of intense vorticity region [21] is similar to that with intense swirlity, and nonvortical flow has a limit in its intensity of $|\omega|$ in this turbulence.

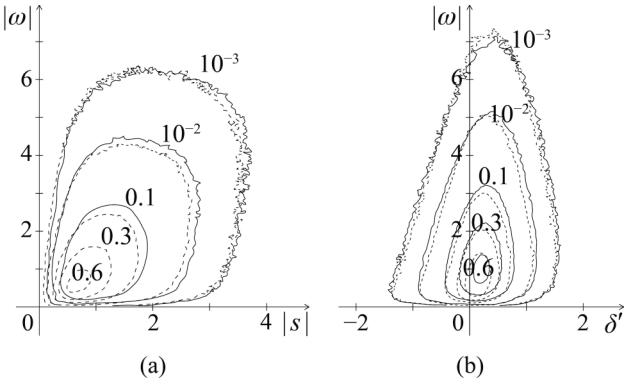

FIG. 3. JPDFs of (a) $(|s|,|\omega|)$ and (b) $(\delta',|\omega|)$, where $\mathrm{Re}_\lambda \approxeq 35$ (solid line) and 51 (dashed line).

In the vortical region where $0 < \phi$, $|\omega|$ and ϕ are almost linearly related. It is noted that, because $\phi < |\omega_3| = |(\alpha + 1/\alpha)\psi|$ (note here $\phi = \psi$), $|\omega|$ is higher than ϕ.

A. Characteristics of vortical structure

Figure 5 shows contours of ϕ and c in the vortical regions where $0 < \phi$, in an instantaneous velocity field where $\mathrm{Re}_\lambda \approxeq 35$. The regions occupied only by the contours of c ($c = 0.75,0.85$), for which ϕ contours ($\phi = 2.5,3$) do not overlap, are vortical regions where ϕ is not as high as those of the contours. A zoomed vortical region in Fig. 5(b) shows that the contour of $\phi = 2.5$ covers that of $\phi = 3$ and those of $c = 0.75$ and 0.85, while the contours of $\phi = 2.5$ and $c = 0.75$ overlap in part. A vortex in this turbulence has a feature of local maximum of ϕ as we raise a threshold of ϕ (ψ) to extract the core region, and c has the similar feature to some extent in its distribution in the cross section of the vortices [22]. Thus both symmetry and swirlity are higher in the core region.

The JPDFs of the data (ε_R,ϕ), (c,ϕ), and (c,ε_R) are shown in Fig. 6. The JPDF of (ε_R,ϕ) indicates that most of the vortices are average-inflow vortices. In high-ϕ regions, these average-inflow vortices are dominant, and $|\varepsilon_R|$ decreases. The JPDF of (c,ε_R) shows that c is concentrated around approximately 0.5. In contrast, the JPDF of the (c,ϕ) indicates that ϕ and c are correlated especially for weak vortices for which $\phi \lessapprox 0.4$, and that ϕ tends to increase with c. Strong (high-ϕ) vortices have high c to some degree, but the increase in c is not as high as that for low-ϕ vortices. Figure 7 shows the flatness f of c for $\phi = 0.1$–2.5, which is high in the low-ϕ region. The reason why the flatness slightly increases for $1 < \phi$ is that the range of c becomes narrow for higher ϕ.

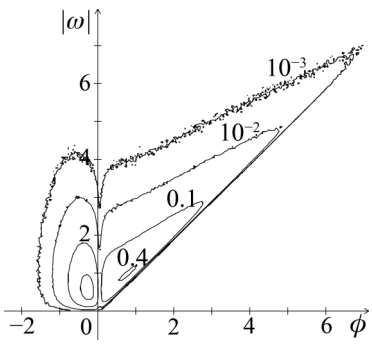

FIG. 4. JPDF of $(\phi,|\omega|)$ (note that $\mathrm{Re}_\lambda \approxeq 35$ hereafter).

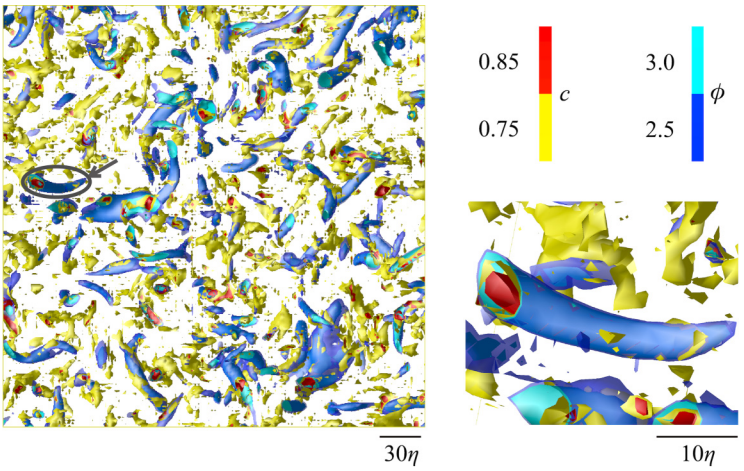

FIG. 5. Contours of ϕ and c where $c = 0.75, 0.85$ and $\phi = 2.5, 3.5$ in an instantaneous velocity field. (a) contours in a subregion and (b) a zoomed vortical region indicated by the arrow in (a).

B. Quantity associated with development/decay of a vortex

The relationships between the time derivatives of ε_R, ϕ, and c are analyzed where the derivatives are estimated by the second-order central difference of time step t in DNS and nondimensionalized by the Kolmogorov time τ. Figure 8 shows the JPDFs of $(\partial c/\partial t, \partial \varepsilon_R/\partial t)$ and $(\partial \varepsilon_R/\partial t, \partial \phi/\partial t)$, for which the correlation coefficients r are -0.042 and 0.087, respectively, and both correlations are low. In contrast, $\partial c/\partial t$ and $\partial \phi/\partial t$ have high correlation, as shown in Fig. 9. Because c and ϕ seem to have a high correlation in the low-ϕ region in Fig. 6, Fig. 9 subdivides the JPDF of $(\partial c/\partial t, \partial \phi/\partial t)$ into low- and (middle) high-ϕ regions to examine differences. A clear correlation is observed between $\partial c/\partial t$ and $\partial \phi/\partial t$ in the low-ϕ region where $\phi < 0.4$, and $\partial c/\partial t$ and $\partial \phi/\partial t$ are statistically proportional. The similar correlation in the transient ϕ and c has been shown by following their time history [23], and this relation is specified clearly with their JPDFs. In the high-ϕ region where $1 < \phi$, they also have a high correlation, and the distribution of the JPDF becomes steep compared with that where $\phi < 0.4$. r in the low- and high-ϕ regions are 0.72 and 0.52, respectively.

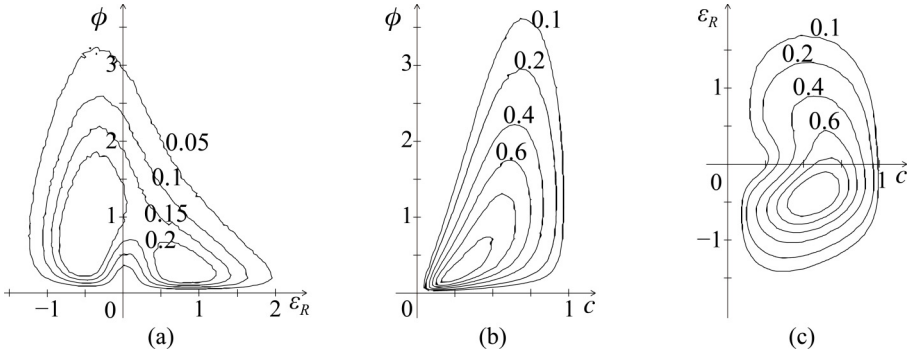

FIG. 6. JPDFs of (a) (ε_R, ϕ), (b) (c, ϕ), and (c) (c, ε_R).

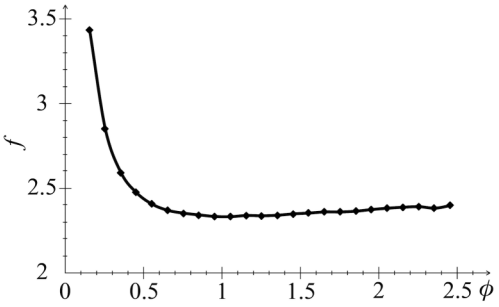

FIG. 7. Flatness (f) of c with respect to ϕ.

C. Vortex stretching and inflow

The JPDF for δ' and ϕ is shown in Fig. 10, which indicates that δ' does not increase in high-ϕ vortices. Figure 11 shows the features of the JPDF for σ and ϕ in average-inflow vortices, i.e., in terms of $\varepsilon_R < 0$. Most of the vortices with inflow are seen to have average inflow ($\sigma < 0$), and the rate of the whole-inflow vortices ($0 < \sigma$) is approximately 15% of the average-inflow vortices. Then a whole-inflow region is located in an average-inflow vortical region and is small [24]. The JPDFs of σ and the components of the vortex stretching $\check{\lambda}'_{r_i}\hat{\omega}_i^2$ ($i = 1,2,3$) or δ' in terms of $\varepsilon_R < 0$ are shown in Fig. 12. Clearly, the whole-inflow vortices have negative terms in $\lambda'_{r_1}\hat{\omega}_1^2$ and $\lambda'_{r_2}\hat{\omega}_2^2$, i.e., compression in all directions in $\mathcal{P}$. However, the average-inflow vortices where $\sigma < 0$ have positive terms in $\lambda'_{r_2}\hat{\omega}_2^2$, and then stretch in the $\boldsymbol{\zeta}_{r_2}$ direction in $\mathcal{P}$. The stretching term $\lambda'_{r_3}\hat{\omega}_3^2 = \varepsilon'_a\hat{\omega}_3^2$ in the direction normal to $\mathcal{P}$ seems to be linear in σ especially in the $0 < \sigma$ region. Moreover, the distribution of $\varepsilon'_a\hat{\omega}_3^2$ in the $0 < \sigma$ region is sharp and steep. This indicates that whole-inflow vortices produce effective stretching rate with less compression (less intensity of radial flow). Even though $|\sigma|$ is the same, $\varepsilon'_a\hat{\omega}_3^2$ with whole inflow is higher than that with average inflow.

V. DISCUSSION

A. Important topological property of a vortex

Figure 13 shows a typical vortical structure derived from Figs. 6 and 11. In the generation of a vortex, ϕ is weak and c is low. It is noted that $c \approx 0$ after the generation. According to development of ϕ, c increases. On the other hand, v_r ($|\lambda_{r_i}|$) or $|\varepsilon_R|$ become weak with the development of ϕ, and σ tends to be negative, thus mixed inflow and outflow exist. In intense vortices, $|\varepsilon_R|$ is much less

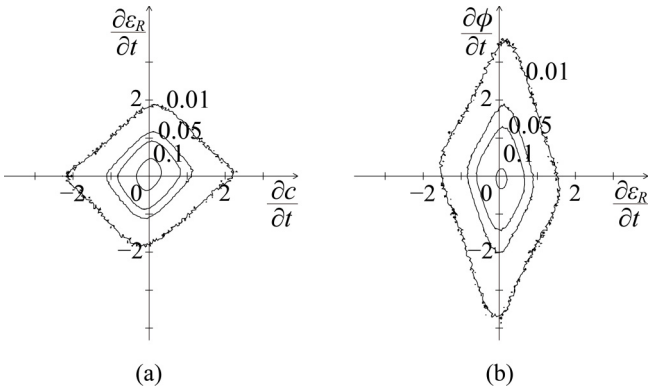

FIG. 8. JPDFs of (a) $(\partial c/\partial t, \partial\varepsilon_R/\partial t)$ and (b) $(\partial\varepsilon_R/\partial t, \partial\phi/\partial t)$.

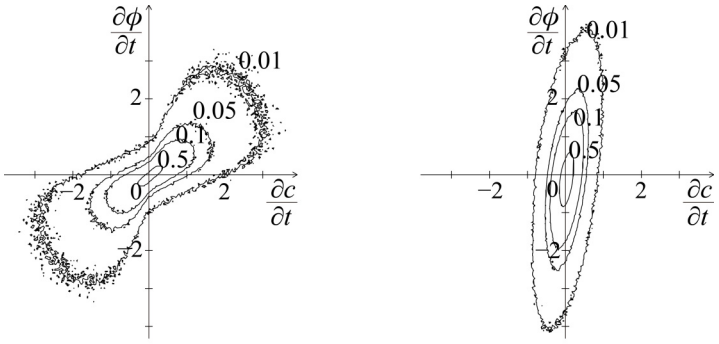

FIG. 9. JPDF of $(\partial c/\partial t, \partial\phi/\partial t)$ in terms of (a) $\phi < 0.4$ and (b) $1 < \phi$.

and $\sigma < 0$, and the vortical flow is almost composed of v_θ. The vorticity components parallel to $\mathcal{P}$, $\hat{\omega}_1$ and $\hat{\omega}_2$, become less as the development of ϕ, because correlation between $|\omega|$ and ϕ becomes high in Fig. 4. Therefore the orthogonality of the vortical axis increases [19]. When a vortex decays, it follows the reverse procedure.

Differently than ε_R, ϕ and c have a strong correlation, and it is stronger in the low-ϕ region with regard to their development or decay. This is a particular feature of the vortex in this turbulence, because increase of c decreases $|\omega|$ mathematically. Since $\breve{\omega}_3 = \hat{\omega}_3 = -(c + 1/c)\phi$ $(\phi = \psi)$, $|\omega|$ effectively increases when c decreases. However, in the development, a vortex or vortical region prefers the increase of both ϕ and c to the decrease of c that leads a skewed vortex. When ϕ increases or forms the local maximum feature in the development, consequently ϕ in surrounding area should increase, for which both intensities of swirl components $\breve{\lambda}_{\theta_1}, \breve{\lambda}_{\theta_2} = -\psi/c, -c\psi$ must increase. For this reason, the increase of c become mandatory. The strong correlation between $\partial c/\partial t$ and $\partial\phi/\partial t$ is derived from the above topological feature. However, their rates depend on the intensity of ϕ, as shown in Fig. 9. When middle- or high-ϕ vortices develop/decay, the corresponding increase/decrease of c is not much, whereas low-ϕ (weak) vortices develop/decay with more change of c. Weak vortices have low c, as shown in Fig. 6(b), and c is zero in the generation/extinction of a vortex. Therefore low-ϕ vortices require more development (or decay) of c than middle-/high-ϕ vortices do. High flatness of c in weak vortices in Fig. 7 indicates this importance for its dynamics. Therefore, c is an important quantity associated with development or decay of ϕ. The swirling motion codevelops or codecays with the vortical flow symmetry, especially for weak vortices.

In vortex stretching, σ classifies the average-inflow or whole-inflow vortices. Whole-inflow vortices decrease $\hat{\omega}_1$ and $\hat{\omega}_2$ ($\breve{\omega}_1$ and $\breve{\omega}_2$), hence $\breve{a}_{13}$ and $\breve{a}_{23}$ in Eq. (11), and therefore increase the

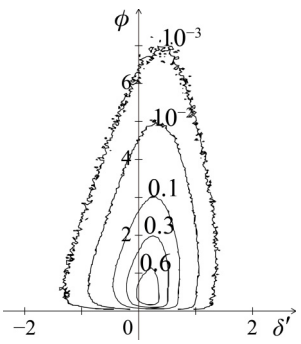

FIG. 10. JPDF of (δ', ϕ).

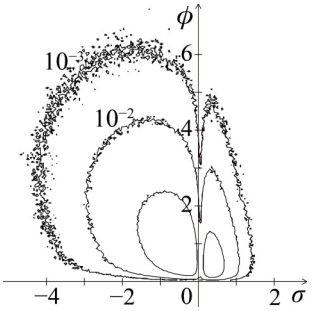

FIG. 11. JPDF of (σ,ϕ) in terms of $\varepsilon_R < 0$ (average-inflow vortices).

orthogonality of the vortical axis $\boldsymbol{\xi}_a$ to $\mathcal{P}$. Figure 12(c) shows that, for whole-inflow vortices with positive σ, even if the inflow (compression) is weak, the stretching rate for $\hat{\omega}_3$ ($\check{\omega}_3$) by the inflow is relatively high. The whole-inflow vortices thus not only improve the orthogonality of the axis, but also efficiently increase vorticity component associated with swirling in terms of flow kinematics.

However, in intense vortices with high ϕ, the correlation between ϕ and c is less, as shown in Figs. 6(b) and 7. To have whole inflow, c must be sufficiently high as ϕ increases, as exhibited by Eqs. (8)–(10). It then makes it difficult for high-ϕ vortices to attain positive σ, which drives the vortex stretching ineffective and thus decreases the orthogonality of the vortical axis. In addition, $|\varepsilon_R| = |\varepsilon_a/2|$ decreases as ϕ increases (Fig. 6), which reduces the rate of stretching. Figure 14 shows a JPDF of ϕ and $|\varepsilon_R|/\phi$ $(0 < \varepsilon_a)$, which exhibits this feature. Figure 1(c) presents a vortical flow geometry of an intense vortex with high ϕ and c but low inflow and negative σ. These topological behaviors suppress the stretching rate in high-ϕ vortices, and are the reason why high intense vortices cannot obtain any effective vortex stretching that strengthens both the swirling intensity (vorticity component normal to $\mathcal{P}$) and the orthogonality of the vortical axis. Therefore, σ is an important

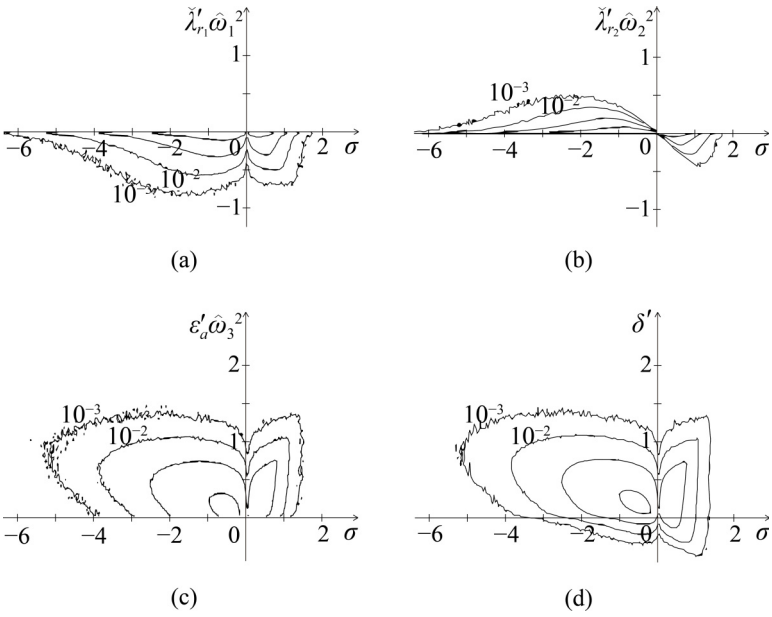

FIG. 12. JPDFs of σ and vortex stretching components, and δ', in terms of $\varepsilon_R < 0$. (a) $(\sigma,\check{\lambda}'_{r_1}\hat{\omega}_1^2)$, (b) $(\sigma,\check{\lambda}'_{r_2}\hat{\omega}_2^2)$, (c) $(\sigma,\varepsilon'_a\hat{\omega}_3^2)$, and (d) (σ,δ').

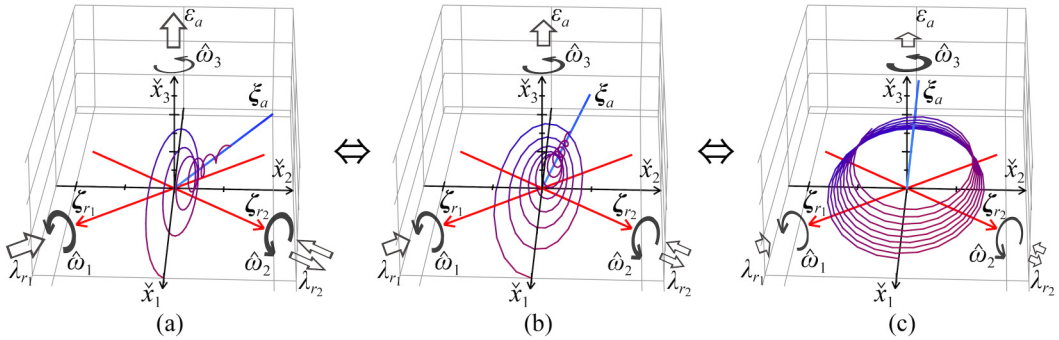

FIG. 13. A model of the life of a vortex. (a) After generation or before extinction with low c and ϕ, (b) developing (or decaying) state with middle c and ϕ, and lower $\hat{\omega}_1$ and $\hat{\omega}_2$, and (c) fully developed with high c and ϕ, and much lower $\hat{\omega}_1$ and $\hat{\omega}_2$, but less stretching rate. $|\lambda_{r_i}|$ (thus ε_a) decreases as ϕ develops, and the sign of $\breve{\lambda}_{r_2}$ and feature of vortex stretching is specified by σ.

quantity associated with supporting the vortical flow structure in terms of the flow kinematics. These features are illustrated in Fig. 13.

Nevertheless, even if ϕ is high and ε_a (or $|\varepsilon_R|$) is small, a vortex can have a positive σ and thus whole inflow when it has a sufficiently high c. Then c is also an important quantity associated with the development/decay of a vortex, whole inflow, and effective vortex stretching, irrespective of the intensity of swirling. Because c is also associated with the development of the pressure minimum of a vortex [19], this symmetry is particularly important in regard to the features of a vortex in terms of the local flow geometry.

As for vortices in other turbulences with different Reynolds numbers, the combined characteristics of (c,ϕ) and its deviation may differ depending on the shear characteristics in the turbulence. However, the development of ϕ requires both $\breve{\lambda}_{\theta_1}$ and $\breve{\lambda}_{\theta_2}$ ($\breve{\lambda}_{\theta_1}$ and $\breve{\lambda}_{\theta_2}$) to increase, and c is given by their ratio in Eq. (7), i.e., $c = (\breve{\lambda}_{\theta_1}/\breve{\lambda}_{\theta_2})^{1/2}$ or $(\breve{\lambda}_{\theta_2}/\breve{\lambda}_{\theta_1})^{1/2}$. Indeed, the development of (only) one $\breve{\lambda}_{\theta_i}$ increases the vorticity component normal to $\mathcal{P}$ because $\omega_s = (\breve{\lambda}_{\theta_1} + \breve{\lambda}_{\theta_2})/2$ from Eq. (7), but it generates a more skewed vortex and does not efficiently increase ϕ. If a vortex has a local maximum feature of ϕ, c should be high because ϕ in surrounding points (in all directions) should be high conformably. If c is low, the high-ϕ region may be restricted in a specific direction. Thus, this primary feature of vortices between c and ϕ may be similar to some extent for those in inhomogeneous or nonisotropic turbulences or in high Reynolds numbers, although the range of c may change according to inhomogeneous or forcing feature in the turbulence. For example, the feature of the local topology in channel turbulence depends on the region or layer to be considered [6]. Even in homogeneous

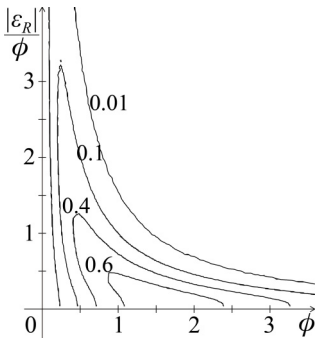

FIG. 14. JPDF of $(\phi,|\varepsilon_R|/\phi)$ in terms of $\varepsilon_R < 0$ $(0 < \varepsilon_a)$.

turbulence, the particular behavior of the intense vorticity region such as layer-like clusters [25] or localization of inhomogeneous feature is observed in high Reynolds number. The flow symmetry in such regions may be restricted by the shear or inhomogeneous characteristics. It is noted that, irrespective of homogeneous/inhomogeneous turbulence, the feature of the local topology depends on the flow feature in the (localized) finite region around the considered point. Then, these features (e.g., flow symmetry, radial/azimuthal flows, vortex stretching) can be analyzed and classified by the present analysis scheme.

On the other hand, vortical structure in terms of the finite scales or multiscales, such as those in the above cluster, is of great interest. If the velocity gradient tensor is given in this scale [26] or by coarse graining [27], then it enables one to analyze the vortical feature of these scales and relationships between their vortical structure in different scales [28]. The details of the transition of the topology or vortex stretching in respective scales can also be specified precisely by the present analysis scheme.

It is a general requirement irrespective of turbulent flows and Reynolds numbers or scales that strong vortices require high symmetry c for whole inflow and effective vortex stretching.

B. Application to realistic vortex models

The present vortical analysis can be applied to other vortices in a variety of turbulent flows encountered in diverse fields from atmospheric physics, with the study of atmospheric vortices, to wind-power engineering and the study of vortices associated with turbines [29,30]. There the analysis is effective in realistic vortex models. As described above, an asymmetric inflow vortex is restricted in terms of a complete inflow region with effective vortex stretching, which can be specified by the sourcity. However, it is noted that, even in the axisymmetric vortex models, the effective stretching region is restricted because the local flow geometry is not axisymmetric except at the center of the vortex. For example, in the Vatistas vortex [31], the radial, azimuthal, and axis velocity components in a cylindrical coordinate system (r, θ, z) are expressed as $u_r = -2(n+1)r^{2n-1}/\{\beta(1+r^{2n})\}$, $u_\theta = r/(1+r^{2n})^{1/n}$, and $u_z = 4n(n+1)r^{2(n-1)}z/\{\beta(1+r^{2n})^2\}$, respectively, where β and n denote a real parameter and positive integer, respectively. In a Cartesian coordinate system x_i $(i = 1,2,3)$, where the x_3 axis coincides with the z axis and $\tan\theta = x_2/x_1$ $(x_1 \neq 0)$, $\nabla \boldsymbol{v}$ in a point in the x_1 axis $(\theta = 0)$ can be expressed in the form

$$\nabla \boldsymbol{v} = \begin{bmatrix} \partial u_r/\partial r & -u_\theta/r & 0 \\ \partial u_\theta/\partial r & u_r/r & 0 \\ \partial u_z/\partial r & 0 & \partial u_z/\partial z \end{bmatrix}, \tag{15}$$

therefore, the local flow geometry is not axisymmetric except at the vortex center $(r = 0)$, and the flow symmetry decreases as r increases. In the $n = 1$ model, the vortical region where $0 < \phi$ $(0 < \Delta)$ is defined by $r_\phi < [1/(1+16/\beta^2)]^{1/4}$, whereas the positive σ region with complete inflow is defined by $r_\sigma < [1/(1+\beta^2/16)]^{1/4}$. They are generally different depending on β for a realistic vortical flow. r_ϕ and r_σ are the same when $\beta = 4$, i.e., $r_\phi = r_\sigma < 0.84$. As β increases however, r_ϕ converges to 1 and r_σ decreases. For example, if $\beta = 8$ then $r_\phi < 0.94$ but r_σ is restricted as $r_\sigma < 0.66$. As the swirling motion is dominant ($|u_\theta|/|u_r|$ increases), the vortical region increases, but the effective stretching region diminishes and is confined. Thus the present analysis provides useful vortical flow characteristics, and sourcity extracts the specific vortical region supported by the flow geometry itself (i.e., effective vortex stretching).

VI. CONCLUSION

The characteristics of the local flow geometry of vortices in an isotropic homogeneous decaying turbulence are clarified, using swirlity, sourcity, and the vortical flow symmetry quantity. Vortex stretching is specified by the quantities associated with the details of the flow geometry.

The development or decay of a vortex in terms of swirlity (intensity of swirling) is associated with the vortical flow symmetry in the swirl plane, especially in weak vortices. Sourcity shows that vortices classified as inflow (convergent) vortices by the complex eigenvalues of the velocity gradient tensor can have both inflow and outflow, which yield vortex stretching in the directions both normal and parallel to the swirl plane and break the orthogonality of the vortical axis to the swirl plane. Vortices with solely inflow in all directions have efficient stretching and an increase in the orthogonality of the vortical axis. Sourcity classifies these characteristics of vortex stretching, and effective stretching requires a positive sourcity and therefore high flow symmetry.

In this regard, the flow symmetry is an important characteristic not only for the development of a vortex but also for complete inflow and an effective stretching. The reason why highly intense vortices cannot undergo such stretching is revealed by the present formulation and the geometrical characteristics of the vortices in this turbulence.

The present analysis provides a detailed topological analysis scheme for vortices in turbulent flows or realistic vortex models, and sourcity extracts the important vortical region supported by its flow kinematics.

ACKNOWLEDGMENT

This study was supported by the 31st Grant from The Nitto Foundation.

[1] T. S. Lundgren, Strained spiral vortex model for turbulent fine structure, Phys. Fluids **25**, 2193 (1982).
[2] H. Tennekes and J. L. Lumley, *A first Course in Turbulence* (MIT Press, Cambridge, MA, 1972).
[3] J. Jiménez, A. A. Wray, P. G. Saffman, and R. S. Rogallo, The structure of intense vorticity in isotropic turbulence, J. Fluid Mech. **255**, 65 (1993).
[4] W. T. Ashurst, A. R. Kerstein, R. M. Kerr, and C. H. Gibson, Alignment of vorticity and scalar gradient with strain rate in simulated Navier-Stokes turbulence, Phys. Fluids **30**, 2343 (1987).
[5] J. Soria, R. Sondergaard, B. J. Cantwell, M. S. Chong, and A. E. Perry, A study of the fine-scale motions of incompressible time-developing mixing layers, Phys. Fluids **6**, 871 (1994).
[6] H. M. Blackburn, N. N. Mansour, and B. J. Cantwell, Topology of fine-scale motions in turbulent channel flow, J. Fluid Mech. **310**, 269 (1996).
[7] M. S. Chong, A. E. Perry, and B. J. Cantwell, A general classification of three-dimensional flow fields, Phys. Fluids A **2**, 765 (1990).
[8] P. Chakraborty, S. Balachandar, and R. J. Adrian, On the relationships between local vortex identification schemes, J. Fluid Mech. **535**, 189 (2005).
[9] J.-Z. Wu, A.-K. Xiong, and Y.-T. Yang, Axial stretching and vortex definition, Phys. Fluids **17**, 038108 (2005).
[10] C. H. Berdahl and D. S. Thompson, Eduction of swirling structure using the velocity gradient tensor, AIAA J. **31**, 97 (1993).
[11] J. Zhou, R. J. Adrian, S. Balachandar, and T. M. Kendall, Mechanisms for generating coherent packets of hairpin vortices in channel flow, J. Fluid Mech. **387**, 353 (1999).
[12] D. Sujudi and R. Haimes, Identification of swirling flow in 3-D vector fields, in *12th Computational Fluid Dynamics Conference*, San Diego, 1995 (AIAA, Reston, VA, 1995).
[13] S. Kida and H. Miura, Identification and analysis of vortical structures, Eur. J. Mech. B/Fluids **17**, 471 (1998).
[14] S. Zhang and D. Choudhury, Eigen helicity density: A new vortex identification scheme and its application in accelerated inhomogeneous flows, Phys. Fluids **18**, 058104 (2006).
[15] K. Nakayama, Physical properties corresponding to vortical flow geometry, Fluid Dyn. Res. **46**, 055502 (2014).

[16] J. C. R. Hunt, A. A. Wray, and P. Moin, Eddies, streams, and convergence zones in turbulent flows, in *Proceedings of the Summer Program 1988* (Center for Turbulence Research, Stanford, 1988), p. 193.
[17] J. Jeong, and F. Hussain, On the identification of a vortex, J. Fluid Mech. **285**, 69 (1995).
[18] K. Nakayama, K. Sugiyama, and S. Takagi, A unified definition of a vortex derived from vortical flow and the resulting pressure minimum, Fluid Dyn. Res. **46**, 055511 (2014).
[19] K. Nakayama, Y. Ohira, and H. Hasegawa, Relationships between local topology of vortical flow and pressure minimum feature derived from flow kinematics in isotropic homogeneous turbulence, J. Fluid Sci. Technol. **11**(1), JFST0007 (2016).
[20] K. Nakayama, Invariant local flow topology in transition into a vortex and property of its prediction, in Proceedings of the 24th International Congress of Theoretical and Applied Mechanics, ICTAM2016, Montreal, No. 129932 (2016).
[21] T. Ishihara, Y. Kaneda, M. Yokokawa, K. Itakura, and A. Uno, Small-scale statistics in high-resolution direct numerical simulation of turbulence: Reynolds number dependence of one-point velocity gradient statistics, J. Fluid Mech. **592**, 335 (2007).
[22] K. Nakayama, Y. Ohira, and S. Yamada, A new parameter in vortex identification and visualization: Symmetry of vortical flow, in *Proceedings of the ASME 2014 International Mechanical Engineering Congress & Exposition*, Montreal, 2014 (ASME, New York, 2014), paper IMECE2014-39859.
[23] K. Nakayama, Y. Ohira, and S. Yamada, An invariant of symmetry of vortical flow, J. Jpn. Soc. Civil Eng. Ser. A2 (Appl. Mech.) **70**(2), I_851 (2014).
[24] K. Nakayama and Y. Ohira, A study of the development and topology of a vortex with inflow in isotropic homogeneous turbulence, Theor. Appl. Mech. Jpn. **63**, 43 (2015).
[25] T. Ishihara, Y. Kaneda, and J. C. R. Hunt, Thin shear layers in high Reynolds number turbulence—DNS results, Flow Turbul. Combust. **91**, 895 (2013).
[26] G. L. Eyink, Multi-scale gradient expansion of the turbulent stress tensor, J. Fluid Mech. **549**, 159 (2006).
[27] T. Ishihara, Y. Yamazaki, and Y. Kaneda, Statistics of small-scale structure of homogeneous isotropic turbulence, in *Proceedings of the IUTAM Symposium on Geometry and Statistics of Turbulence*, Kanagawa, 1999, edited by T. Kambe, T. Nakano, and T. Miyauchi, Fluid Mechanics and Its Applications Vol. 59 (Springer, Netherlands, 2001).
[28] J. C. R. Hunt, T. Ishihara, N. A. Worth, and Y. Kaneda, Thin shear layers in high Reynolds number turbulence - Tomographic experiments and a local distortion model, Flow Turbul. Combust. **92**, 607 (2014).
[29] V. T. Wood and L. W. White, A new parametric model of vortex tangential-wind profiles: Development, testing, and verification, J. Atmos. Sci. **68**, 990 (2011).
[30] M. Dreyer, J. Decaix, C. Münch-Alligné, and M. Farhat, Mind the gap: A new insight into the tip leakage vortex using stereo PIV, Exp. Fluids **55**, 1849 (2014).
[31] G. H. Vatistas, New model for intense self-similar vortices, J. Prop. Power **14**, 462 (1998).